

Compact in-vacuum gamma-ray spectrometer for high-repetition rate PW-class laser-matter interaction

G. Fauvel,^{1,2} K. Tangtharakul,³ A. Arefiev,³ O. Klimo,² M. Manuel,⁴ P. Rubovic,¹ S. Weber,¹ and F.P. Condamine¹

¹*ELI Beamlines Facility\The Extreme Light Infrastructure ERIC Za Radnicí 835, 252 41 Dolní Břežany, Czech Republic*

²*Czech Technical University in Prague, Faculty of Nuclear Sciences and Physical Engineering , 115 19, Czech Republic*

³*Center for Energy Research, University of California San Diego, La Jolla, CA 92093, USA*

⁴*General Atomics, San Diego, CA 92186, USA*

(*Electronic mail: Gaetan.Fauvel@eli-beams.eu)

(Dated: 21 November 2023)

With the advent of high repetition rate laser facilities, novel diagnostic tools compatible with these advanced specifications are in demand. This paper presents the design of an active gamma-ray spectrometer intended for these high repetition rate experiments, with particular emphasis on functionality within a PW level laser-plasma interaction chamber's extreme conditions. The spectrometer uses stacked scintillators to accommodate a broad range of gamma-ray energies, demonstrating its adaptability for various experimental setups. Additionally, it has been engineered to maintain compactness, electromagnetic pulse resistance, and ISO-5 cleanliness requirements while ensuring high sensitivity. The paper also outlines the unfolding process to recover the gamma-ray spectrum from the spectrometer's captured image thanks to a calibration using a ⁶⁰Co radioactive source.

I. INTRODUCTION

In recent years, advancements in laser technology across the globe have led to an increase not only in power levels but also in repetition rates. Presently, several facilities are capable of delivering PW class laser pulses at intervals of a few minutes to seconds¹⁻⁴. For instance, the L3 laser at ELI Beamlines in Czech Republic can generate 0.5 PW shots at a frequency of 3.3 Hz. Similarly, the BELLA center in the USA can reach 0.5 PW shots at a frequency of 10 Hz³. This surge in statistical data presents exciting opportunities for the plasma community, but it also necessitates corresponding advancements in diagnostic tools.

It is crucial that detectors are compatible with the new energy ranges of produced particles⁵⁻¹⁰ at these new intensity levels. In this range, the gamma-ray photons produced can provide insights into topics like the production of gamma-ray bursts in astrophysics^{11,12}, radioactive waste management¹³, and the production of matter through photon-photon collision as theorized by Breit-Wheeler¹⁴⁻¹⁶. There is also significant industry interest in reliably and well-characterized production of high energy photons, which can traverse matter more efficiently and be used as non-destructive probes^{17,18}.

While several methods exist to produce high energy photons^{13,19-23}, a recent method known as Direct Laser Acceleration (DLA) method^{8,24} has promising laser to photon conversion in the range of several percents with a low divergence of gamma-ray emission. This method involves accelerating electrons to relativistic speed in a near-critical density target due to the ponderomotive force. The electrons produce a quasi-static azimuthal magnetic field due to a return current, and thanks to their oscillation within the high-intensity laser beam, they undergo oscillations generating photons by Compton scattering. This leads to a bright, collimated syn-

chrotron emission-like of high-energy gamma-rays. At PW levels, gamma-rays up to a few MeV (for 0.5PW lasers) to hundreds of MeV (for 10PW lasers) can be produced^{8,25}.

In order to conduct these experiments, we need to design a diagnostic tool suitable for these high energies. Current designs are sufficient and adaptable for charged particles^{26,27}. However, for photons existing designs, such as those for X-ray spectrometers using diffraction^{28,30}, cannot be directly applied as no crystals have a small enough interplanar spacing to diffract these wavelength (0.1 Å). We therefore need a new type of detector. This new energy range has been under exploration for several years, and corresponding detectors have been developed³¹⁻³⁷. These detectors utilize a pattern of alternating absorbers and Imaging Plates (IPs). By adjusting the thickness and material type of the absorbers, the energy spectrum can be unfolded. However, these stacking calorimeters have a significant limitation linked to the passivity of the detector. IPs must be analyzed between shots, a time-consuming process reducing the advantage of new high-repetition rate lasers without accumulating over several shots.

In response to this challenge, several research groups have developed active gamma-ray spectrometer designs^{38,39}. By operating as both absorbers and detectors simultaneously, scintillators uphold the principle of energy deposition variation while also ensuring compactness and sensitivity. These spectrometers are usually located outside the interaction chamber, with the stack of scintillators placed directly behind a Beryllium window or a thick aluminum flange. However this additional obstacle can emit supplementary radiation or particles creating difficulties in retrieving the original spectrum. By positioning the spectrometer inside the chamber, we can strongly reduce this parasitic signal.

Besides, as interaction chambers continue to increase in size, centimeter-scale scintillators fail to cover the entire

opening angle of the gamma rays, which is typically from 30° (~ 500 mrad) for low energy photons to few degrees (~ 150 mrad) for the highest energy photons, as predicted for gamma flash experiments²⁴. Although increasing the size of the scintillators is an option, it is impractical to create very large windows due to pressure and costs constraints. Additionally, this reduces the spectrometer's adaptability to position as the angular position will be only defined by the position of flanges and/or windows around the interaction chamber. As a result, we decided to focus on designing a spectrometer that can fit inside the experimental chamber. But, operating within the confines of an interaction chamber presents its own set of unique challenges, most notably the reduced available space. The chamber often houses multiple components such as large optics which can significantly limit the available real space for additional devices like detectors. To address this, we introduce a highly compact gamma-ray spectrometer in this paper. The spectrometer has been engineered with dimensions of $20 \times 20 \times 25 \text{ cm}^3$, making it particularly well-suited for high-repetition-rate experiments and adaptable to the rigorous environmental conditions characteristics of a laser-plasma interaction chamber (EMPs, cleanliness, vacuum pressure, etc.).

This manuscript describes the design of the high repetition rate spectrometer suited for the extreme constraints of the PW-level interaction chamber in Section II. Section III elaborates on the methodology employed for unfolding the gamma-ray spectrum from the acquired spectrometer images. This process is crucial for translating the raw data into meaningful energy spectrum. The paper follows with a discussion of the calibration process, outlining the strategies employed to align the experimental setup with the theoretical models.

II. DESIGN OF A GAMMA-RAY SPECTROMETER WITH STACKING SCINTILLATORS

In this manuscript, gamma rays are classified as photons with energy > 100 keV. To accommodate these high energies, the fluorescence properties of various materials can be used. Gamma-ray photons deposit some of their energy within these materials, thereby exciting them. The materials subsequently relax, emitting fluorescence photons generally within the optical energy range. This allows the use of an optical Charge-Coupled Device (CCD) to collect them. By arranging scintillators in a stack configuration in the laser axis, the first layers act as detectors for lower energy gamma rays and at the same serve as a filter allowing for the detection of only (ideally) higher energy gamma-rays in the deeper scintillators.

Energy deposition is primarily dependent on three factors: the energy of the incident photon, the material of the scintillator, and its thickness. As we aim to determine the photon, we have two adjustable parameters: the material and the thickness of the scintillator. Different types of scintillators offer different absorption coefficients for varying gamma-ray energies. The spectrometer designed in this study is intended to be used in different experimental setups covering different energy ranges. Consequently, we employ various types of scintillators to widen the energy range. The stack uses three

different types of scintillators with various thicknesses related to their absorption coefficients. Plastic scintillators possess a low absorption coefficient, facilitating the detection of photons below 100 keV ⁴⁰. YAG:Ce scintillators are more suitable for detection in the MeV range⁴¹, and finally, CsI:Tl scintillators are ideal for energies above 5 to 10 MeV ⁴². The limited space within most chambers led us to use a limited number of scintillators, in a layered configuration of scintillators adapted to the expected gamma-ray spectrum. Here the configuration includes two 2 cm thick vinyltoluene (plastic) scintillators, ten 5 mm thick YAG:Ce scintillators, and five 5 mm thick CsI:Tl scintillators, all furnished by Advatech UK Ltd. The arrangement of the scintillators is illustrated in Fig. 1. Note that this modular design allows for the individual scintillators to be readily interchanged, offering flexibility to accommodate a range of energy spectra as necessitated by different experimental requirements. The design prioritizes compactness to facilitate integration with various experimental setups. Nevertheless, this compactness comes at the cost of a fixed configuration's versatility. To mitigate this, one could envisage a spectrometer with a larger number of scintillators.

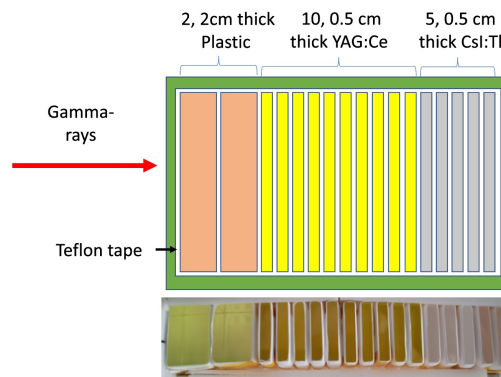


FIG. 1: Scheme of the scintillator at the top and physical stack at the bottom. Each scintillator has the same transversal and vertical dimensions of 5cm each, only the thickness varies. TeflonTM tape is wrapped around each scintillator to increase photon collection, avoid the overlap of signals (optical photons going out through an adjacent scintillator) and allow some spatial separation for the CCD acquisition.

A critical factor in the spectrometer's performance is the decay time of the scintillators, particularly the CsI:Tl, which has the longest decay time of 900 ns. This characteristic time can limit maximum repetition rate that can be used without signal overlap. Even if the scintillator hardware is far above the required characteristics, the camera becomes the limiting factor for the repetition rate achievable. As an example the camera used here from Allied Vision, model "Manta Camera 507-B", can only reach up to 23 fps but can be easily fixed with a high speed camera. With the current setup operating at a repetition rate of 10 Hz, the system is within the limits, ensuring clear temporal separation of detection events.

The fluorescence photons from the scintillators are collected using an optical CCD combined with an f/1.8 objective to have a large field of view with a short focal distance

as the spectrometer height is only 20 cm. Each scintillator is wrapped in TeflonTM tape, leaving one polished face exposed, to enhance photon collection towards the CCD while maintaining sufficient spatial spacing for scintillator differentiation. To shield the CCD from Electromagnetic Pulses (EMPs) emitted during laser-plasma interaction, a 5 mm copper Faraday cage is installed around it. To protect the CCD from the plasma self-emission (and any other parasitic light), a box composed of 2 mm aluminium sheets held by 90° clamps is positioned around the spectrometer. Using appropriate opto-mechanical elements, we meet cleanliness requirements, achieving a pressure of $10^{-6} \pm 10^{-7}$ mbar inside the interaction chamber and passing Residual Gas Analysis (RGA) tests. The spectrometer's assembly, suited for installation within the chamber, is presented in Fig. 2.

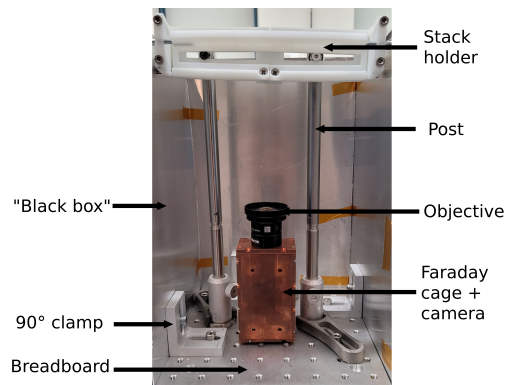


FIG. 2: Spectrometer's assembly suited for installation inside a PW-class laser interaction chamber. One side and top panels have been removed for clarity. Stack configuration is presented in Fig. 1

Having underlined the hardware components of the detection system, attention must now turn to the process of data interpretation. The raw data captured by the CCD requires a transformation to yield a meaningful gamma-ray spectrum. This transformation process, commonly referred to as "unfolding," is essential to convert the digitized image data into a physically interpretable format. Unfolding is a pivotal step in the experimental pipeline as the quality of the algorithm directly impacts the accuracy and resolution of the resultant gamma-ray spectrum, thereby influencing the interpretation of the underlying physical phenomena. Given the complexity of the data and the risk for various sources of noise and distortion, the algorithm applied must be robust and meticulously validated to ensure reliable results. The method is presented in the next section.

III. METHODOLOGY FOR UNFOLDING

In order to accurately reconstruct the energy spectrum of the particle source under investigation, several computational and data analysis techniques must be employed on the data captured by the spectrometer. One of the primary outputs

from the spectrometer is the image, which is acquired using a CCD camera. This scintillation image serves as a raw source of information and is directly correlated to the energy deposited within various scintillation materials. It should be noted that the energy deposition is a function of not only the particles' inherent energy and type but is also modulated by a set of factors collectively termed as the "relative light yield."

The concept of relative light yield (RLY) is a composite parameter that includes a variety of conversion factors, each contributing to the overall signal transformation process from the FLUKA output to a CCD pixel value equivalent. These factors are the intrinsic light yield of the scintillation materials utilized directly dependant on the material but can also vary depending on the manufacturing of the scintillator crystal. The angular dependencies affecting photon collection efficiencies for example scintillators on the left of the image will have less photons collected by the objective than the scintillators in the center (for a same initial emission). The quantification efficiency of the CCD camera, which is responsible for converting the collected photons into a digitized pixel array. This overall factor allows a simple linear relationship between the FLUKA output and the CCD value. This parameter, unique for each scintillator, is defined through the calibration process, detailed in Section IV, thereby enabling the conversion of the scintillation image to meaningful particle energy. Equation 1 is a simple equation for this RLY parameter, using η_i as all the possible conversion which contribute to the final pixel value. The RLY is defined as η_{RLY} , the CCD pixel value is noted E_{CCD} and the FLUKA output is noted E_{FL} .

$$\text{CCD pixel value} = \text{FLUKA output} \times \sum \text{Conversion factors}$$

$$E_{CCD} = E_{FL} \times \sum_i \eta_i = E_{FL} \times \eta_{RLY}$$

$$\text{Relative light yield (RLY)} = \sum \text{Conversion factors}$$

$$\eta_{RLY} = \sum_i \eta_i \quad (1)$$

To calculate the energy deposition in the scintillators, we employ a Monte Carlo simulation approach using the FLUKA code^{43,44}. This is complemented by the FLAIR software⁴⁵ a visual interface used that serves as an interface for effectively configuring and visualizing the FLUKA simulations. Together, they provide a robust framework for simulating the experimental setup in a virtual environment, thereby allowing us to account for material-specific interactions, scattering, and other complex phenomena that influence the observed data.

Once the simulation environment is established, the energy spectrum of the particle source is iteratively adjusted. The aim is to minimize the divergence between the simulated and experimental data, subject to the modulation imposed by the RLY of the scintillators used. It is critical to note that while this is a widely used approach, alternative methodologies exist that might offer advantages in specific applications. For instance, machine learning techniques like neural networks or statistical methods such as Bayesian unfolding algorithms can also be employed to decode the energy spectrum. Although

these advanced techniques are beyond the scope of this work, they represent important directions for future research. A typical equation used to simulate the photon spectra is a synchrotron distribution

$$S(x) = x \int_x^{+\infty} K_{\frac{5}{3}}(\chi) d\chi \quad (2)$$

, with $x = \frac{E}{E_c}$ and E_c the critical energy and $K_\alpha(x)$ the modified Bessel function of order α at the point x . When considering the electron acceleration we obtain the equation :

$$S(x) = x^2 \int_{-1}^1 \left(\frac{1}{(1-\mu^2)^{\frac{3}{2}}} K_{\frac{2}{3}}(x(1-\mu^2)^{-\frac{7}{4}})^2 d\mu \right) \quad (3)$$

To further account for Bremsstrahlung-like emission, an exponential spectrum can be used as follows:

$$S(E) = \sqrt{E} e^{-\frac{E}{k_B T}} \quad (4)$$

Here, $k_B T$ represents the effective temperature of the photon distribution in eV.

The validation of the unfolding algorithm's accuracy is contingent upon the availability of empirical data. The algorithm's consistency is evaluated through a calibration process that determines the conversion factor between the energy deposited inside the scintillators and the CCD value. This calibration not only serves to fine-tune the system's response but also provides a basis for assessing the algorithm's precision. By employing this real-world data, one can benchmark the algorithm's performance, ensuring that the derived gamma-ray spectrum accurately reflects the physical event. The calibration data thus plays a dual role: it helps in the optimization of the light yield measurements and furnishes a metric against which the unfolding algorithm's accuracy is gauged.

IV. CALIBRATION USING A ^{60}Co RADIOACTIVE SOURCE

The task of calibrating a stacked gamma-ray spectrometer is a complex challenge that necessitates meticulous planning and resource allocation. One of the most critical requirements for calibration is the selection of an appropriate radiation source. The ideal source should possess a well-defined and accurate energy spectrum, with photon energies exceeding the 500 keV range and a sufficiently high photon flux to ensure statistical reliability.

In our specific case, we opted to use sources with activities in the TBq range. After careful consideration, a ^{60}Co source was selected for its suitability for our experiment. This source has an activity of 0.185 TBq and emits photons with two dominant photopeaks at energies of 1.173 MeV and 1.332 MeV. The experimental setup was configured at a distance of 1 m from the source which has an opening angle of 11° (~ 200 mrad).

Data acquisition was executed under varying conditions of gain and exposure time to optimize the sensitivity and dynamic range of the CCD camera. A typical scintillation image obtained from this setup is shown in Fig. 3.

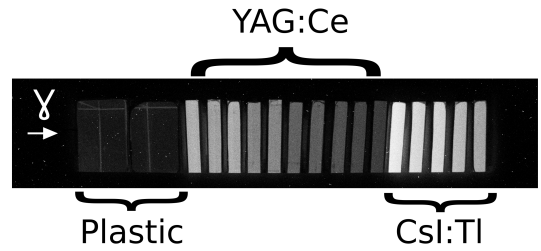


FIG. 3: Observed image using a ^{60}Co calibration source at 1m of the detector. 40 Gain and 0.5s exposure time. Three different type of scintillators are used, explaining the abrupt changes in scintillation along the propagation axis. Radiation comes from the left with the source at 1m with an opening angle of 11° . Contrast was enhanced for better visibility

Upon the successful completion of the data acquisition phase, we proceeded to start the comparative analysis between our experimentally derived data and the simulations generated from FLUKA. This meticulous comparison was critical for the extraction of the RLY key metric defined in Equation 1.

To further refine the data and mitigate inconsistencies or inhomogeneities, we applied a statistical treatment to the acquired pixel values. Specifically, the mean pixel value was calculated for each individual scintillator in the stacked array. This process effectively smoothen the data, making it easier to directly compare with simulation outputs. The processed mean pixel values are plotted against the FLUKA simulation results, as illustrated in Fig. 4.

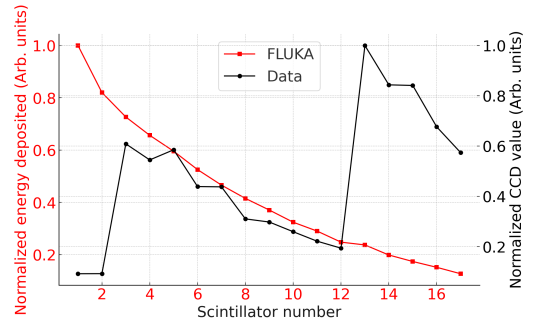


FIG. 4: Comparison between CCD output image and FLUKA simulation for a 0.185 TBq ^{60}Co calibration source. Both FLUKA and CCD outputs are normalized.

It is now possible to compute the RLY, normalized and averaged across specimens of each scintillator type, are presented as follows: for the plastic scintillators, $(2.3 \pm 0.3) \times 10^{-2}$; for YAG:Ce, $(1.87 \pm 0.1) \times 10^{-1}$; and for CsI:Tl, (1 ± 0.1) in units of GeV. These quantifications, which represent the photon-to-light conversion efficiency, are crucial for the accurate interpretation of the energy spectrum deduced from the observed data. This means that every FLUKA output will be multiplied by the relative light yield specific to each scintillator before trying to compare it to the experimental data.

In order to use this unfolding algorithm it is necessary to simulate a fixed spectrum, look at the FLUKA output and

compare to the experimental data. To simulate the spectrum it is necessary to create it using an equation. However equations might not always represent the actual signal measured (Double population of photons, different particles, etc.). In order to check the impact of the simulated spectrum by an equation, we compare it to the actual spectrum generated by the source. A Gaussian shape aimed to represent the photopeaks of the radioactive source are simulated. The best fit corresponding to a gaussian shape centered at 1.7 MeV with a width at $\frac{1}{2}$ of 0.5 MeV is presented in Fig. 5.

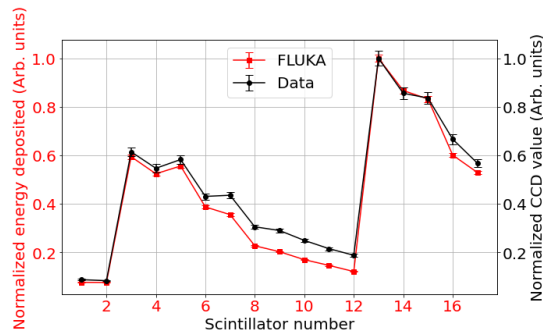


FIG. 5: Comparison between CCD output image obtained from a 0.185 TBq ^{60}Co calibration source and FLUKA simulation from a gaussian distribution of photons centered at 1.7 MeV of width 0.5 MeV. Both FLUKA and CCD outputs are normalized.

Thus the analysis reveals that the unfolding algorithm is unable to accurately resolve the dual photopeak structure, and exhibits a systematic shift in the energy spectrum. This discrepancy arises primarily from two factors. Firstly, the inherent resolution of the spectrometer constrains its ability to distinguish between peaks that are in close proximity, such as the observed 1.173 MeV and 1.332 MeV peaks. The spectrometer's design does not cater to the high precision required to differentiate between energy levels that are closely spaced.

Secondly, the source itself contributes to the deviation. The emission includes not only the desired photons but also electrons and lower-energy photons. These additional particles interact with the scintillator material, depositing energy and thereby introducing extraneous signals into the measured spectrum. Using the entirety photon spectrum emitted by the radioactive source which includes lower energy photon photons (Bremsstrahlung, etc.) we are able to almost perfectly match the data as presented in Fig. 6. Consequently, it becomes imperative to have a comprehensive understanding of the spectrum of other particles that could potentially interact with the scintillators and the generating process of the gamma-ray emission to orientate fitting simulations. Note that the match is not perfect as the radioactive source also emits low energy electrons which are not included here.

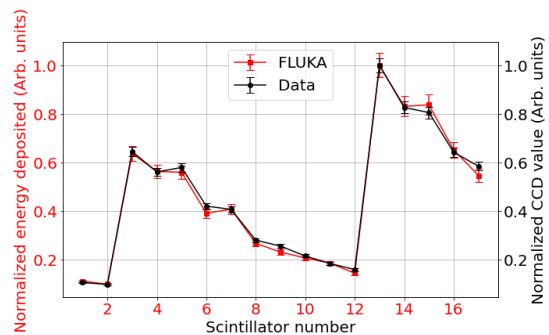


FIG. 6: Comparison between CCD output image obtained from a 0.185 TBq ^{60}Co calibration source and FLUKA simulation from theoretical photon emission spectrum of a ^{60}Co source. Both FLUKA and CCD outputs are normalized.

V. DISCUSSION

To conclude, in this manuscript an active gamma-ray spectrometer suited for PW-class laser interaction chamber is presented for gamma-rays detection from 100 keV to 10 MeV. This spectrometer offers several advantages in its design. First by using a stack of different scintillators it can reach high repetition rate of up to 10 Hz which can be easily increased by upgrading the camera model to a faster camera. This design is modular meaning each scintillator can be easily replaced or swapped to meet the needs of energy analysis, precision or maintenance.

The spectrometer's compatibility with the rigorous demands of a PW-class laser interaction chamber, such as electromagnetic pulse (EMP) resistance, vacuum pressure tolerance, and maintenance of cleanliness, is ensured through a careful selection of materials and design.

It is mandatory to couple this spectrometer with an electron spectrometer. The latter serves as a magnetic field source to deflect electrons and also provides more accurate data regarding the contribution of electrons to the overall signal.

This spectrometer will be implemented in experiments for gamma-ray studies at ELI-Beamlines in the Experimental Hall E3. The robust design is believed to be able to withstand the 10 PW-class laser L4f and PW-class laser L3 of respective repetition rate 0.016 Hz and 10 Hz. The detection of high energy gamma-rays at such high repetition rate will allow the plasma community to have insightful data and statistics to study unresolved phenomena like gamma-ray bursts in astrophysics or understand efficient gamma-ray generation parameters for example in DLA.

ACKNOWLEDGMENTS

We would like to thank V. Istokskaia, L. Giuffrida and B. Lefebvre, R. Versaci, C. Lacoste, for fruitful conversation regarding the design and unfolding method. We would like to also thank The National Radiation Protection Institute (NRPI) in Prague, Cz for their help in the calibration process. We wish

to acknowledge the support of the National Science Foundation (NSF) and Grantová agentura České republiky (GAČR) for funding on project number No. 22-42890L.

DATA AVAILABILITY STATEMENT

The data that support the findings of this study are available from the corresponding author upon reasonable request.

REFERENCES

- ¹D. Doria, M. Cernaianu, P. Ghenuche, D. Stutman, K. Tanaka, C. Ticos, and C. Ur, *Journal of Instrumentation* **15**, C09053 (2020).
- ²K. Burdonov, A. Fazzini, V. Lelasseux, J. Albrecht, P. Antici, Y. Ayoul, A. Beluze, D. Cavanna, T. Ceccotti, M. Chabanis, A. Chaleil, S. N. Chen, Z. Chen, F. Consoli, M. Cuciuc, X. Davoine, J. P. Delaneau, E. d’Humières, J.-L. Dubois, C. Evrard, E. Filippov, A. Freneaux, P. Forestier-Colleoni, L. Gremillet, V. Horny, L. Lancia, L. Lecherbourg, N. Lebas, A. Leblanc, W. Ma, L. Martin, F. Negoita, J.-L. Paillard, D. Papadopoulos, F. Perez, S. Pikuz, G. Qi, F. Quééré, L. Ranc, P.-A. Söderström, M. Scisciò, S. Sun, S. Vallières, P. Wang, W. Yao, F. Mathieu, P. Audebert, and J. Fuchs, *Matter and Radiation at Extremes* **6**, 064402 (2021).
- ³S. Hakimi, L. Obst-Huebl, A. Huebl, K. Nakamura, S. S. Bulanov, S. Steinke, W. P. Leemans, Z. Kober, T. M. Ostermayr, T. Schenkel, A. J. Gonsalves, J.-L. Vay, J. van Tilborg, C. Toth, C. B. Schroeder, E. Esarey, and C. G. R. Geddes, *Physics of Plasmas* **29**, 083102 (2022).
- ⁴L. Volpe, R. Fedosejevs, G. Gatti, J. A. Pérez-Hernández, C. Méndez, J. Apiñaniz, X. Vaisseau, C. Salgado, M. Huault, S. Malko, G. Zeraouli, V. Ospina, A. Longman, D. D. Luis, K. Li, O. Varela, E. García, I. Hernández, J. D. Pisonero, J. G. Ajates, J. M. Alvarez, C. García, M. Rico, D. Arana, J. Hernández-Toro, and L. Roso, *High Power Laser Science and Engineering* **7**, e25 (2019), publisher: Cambridge University Press.
- ⁵C. P. Ridgers, C. S. Brady, R. Ducloux, J. G. Kirk, K. Bennett, T. D. Arber, A. P. L. Robinson, and A. R. Bell, *Physical Review Letters* **108**, 165006 (2012), publisher: American Physical Society.
- ⁶X.-L. Zhu, T.-P. Yu, Z.-M. Sheng, Y. Yin, I. C. E. Turcu, and A. Pukhov, *Nature Communications* **7**, 13686 (2016), number: 1 Publisher: Nature Publishing Group.
- ⁷P. A. Norreys, *Nature Photonics* **3**, 423 (2009), number: 8 Publisher: Nature Publishing Group.
- ⁸O. Jansen, T. Wang, D. J. Stark, E. d’Humières, T. Toncian, and A. V. Arefiev, *Plasma Physics and Controlled Fusion* **60**, 054006 (2018), publisher: IOP Publishing.
- ⁹A. Higginson, R. J. Gray, M. King, R. J. Dance, S. D. R. Williamson, N. M. H. Butler, R. Wilson, R. Capdessus, C. Armstrong, J. S. Green, S. J. Hawkes, P. Martin, W. Q. Wei, S. R. Mirfayzi, X. H. Yuan, S. Kar, M. Borghesi, R. J. Clarke, D. Neely, and P. McKenna, *Nature Communications* **9**, 724 (2018), number: 1 Publisher: Nature Publishing Group.
- ¹⁰M. Jirka, O. Klimo, M. Vranic, S. Weber, and G. Korn, *Scientific Reports* **7**, 15302 (2017), number: 1 Publisher: Nature Publishing Group.
- ¹¹T. Piran, *Reviews of Modern Physics* **76**, 1143 (2005), publisher: American Physical Society.
- ¹²P. Mészáros, *Reports on Progress in Physics* **69**, 2259 (2006).
- ¹³J. Galy, M. Maučec, D. J. Hamilton, R. Edwards, and J. Magill, *New Journal of Physics* **9**, 23 (2007).
- ¹⁴G. Breit and J. A. Wheeler, *Physical Review* **46**, 1087 (1934), publisher: American Physical Society.
- ¹⁵K. Krajewska and J. Z. Kamiński, *Physical Review A* **86**, 052104 (2012), publisher: American Physical Society.
- ¹⁶T. G. Blackburn and M. Marklund, *Plasma Physics and Controlled Fusion* **60**, 054009 (2018), publisher: IOP Publishing.
- ¹⁷A. Ben-Ismaïl, O. Lundh, C. Rechatin, J. K. Lim, J. Faure, S. Corde, and V. Malka, *Applied Physics Letters* **98**, 264101 (2011).
- ¹⁸Y. C. Wu, B. Zhu, G. Li, X. H. Zhang, M. H. Yu, K. G. Dong, T. K. Zhang, Y. Yang, B. Bi, J. Yang, Y. H. Yan, F. Tan, W. Fan, F. Lu, S. Y. Wang, Z. Q. Zhao, W. M. Zhou, L. F. Cao, and Y. Q. Gu, *Scientific Reports* **8**, 15888 (2018), number: 1 Publisher: Nature Publishing Group.
- ¹⁹A. Giulietti, N. Bourgeois, T. Ceccotti, X. Davoine, S. Dobosz, P. D’Oliveira, M. Galimberti, J. Galy, A. Gamucci, D. Giulietti, L. A. Gizzi, D. J. Hamilton, E. Lefebvre, L. Labate, J. R. Marquès, P. Monot, H. Popescu, F. Réau, G. Sarri, P. Tomassini, and P. Martin, *Physical Review Letters* **101**, 105002 (2008), publisher: American Physical Society.
- ²⁰K. W. D. Ledingham and W. Galster, *New Journal of Physics* **12**, 045005 (2010).
- ²¹J. Cole, K. Behm, E. Gerstmayr, T. Blackburn, J. Wood, C. Baird, M. Duff, C. Harvey, A. Ilderton, A. Joglekar, K. Krushelnick, S. Kuschel, M. Marklund, P. McKenna, C. Murphy, K. Poder, C. Ridgers, G. Samarín, G. Sarri, D. Symes, A. Thomas, J. Warwick, M. Zepf, Z. Najmudin, and S. Mangles, *Physical Review X* **8**, 011020 (2018), publisher: American Physical Society.
- ²²E. N. Nerush, I. Y. Kostyukov, L. Ji, and A. Pukhov, *Physics of Plasmas* **21**, 013109 (2014).
- ²³E. N. Nerush and I. Y. Kostyukov, *Plasma Physics and Controlled Fusion* **57**, 035007 (2015), publisher: IOP Publishing.
- ²⁴D. Stark, T. Toncian, and A. Arefiev, *Physical Review Letters* **116**, 185003 (2016).
- ²⁵S. Li, B. Shen, J. Xu, T. Xu, Y. Yu, J. Li, X. Lu, C. Wang, X. Wang, X. Liang, Y. Leng, R. Li, and Z. Xu, *Physics of Plasmas* **24**, 093104 (2017).
- ²⁶K. Nakamura, W. Wan, N. Ybarrolaza, D. Syversrud, J. Wallig, and W. P. Leemans, *Review of Scientific Instruments* **79**, 053301 (2008).
- ²⁷R. Faccini, F. Anelli, A. Bacci, D. Batani, M. Bellaveglia, R. Benocci, C. Benedetti, L. Cacciotti, C. A. Cecchetti, A. Clozza, L. Cultrera, G. Di Pirro, N. Drenska, M. Ferrario, D. Filippetto, S. Fioravanti, A. Gallo, A. Gamucci, G. Gatti, A. Ghigo, A. Giulietti, D. Giulietti, L. A. Gizzi, P. Koester, L. Labate, T. Levato, V. Lollo, P. Londrillo, S. Martellotti, E. Pace, N. Patack, A. Rossi, F. Tani, L. Serafini, G. Turchetti, C. Vaccarezza, and P. Valente, *Nuclear Instruments and Methods in Physics Research Section A: Accelerators, Spectrometers, Detectors and Associated Equipment Irs International Conference on Frontiers in Diagnostics Technologies*, **623**, 704 (2010).
- ²⁸B. K. F. Young, A. L. Osterheld, D. F. Price, R. Shepherd, R. E. Stewart, A. Y. Faenov, A. I. Magunov, T. A. Pikuz, I. Y. Skobelev, F. Flora, S. Boltanti, P. Di Lazzaro, T. Letardi, A. Grilli, L. Palladino, A. Reale, A. Scafati, and L. Reale, *Review of Scientific Instruments* **69**, 4049 (1998).
- ²⁹N. M. Ceglio, R. L. Kauffman, A. M. Hawryluk, and H. Meddecki, *Applied Optics* **22**, 318 (1983), publisher: Optica Publishing Group.
- ³⁰W. H. Bragg and W. L. Bragg, *Proceedings of the Royal Society of London. Series A* **88**, 428 (1913).
- ³¹A. Hannasch, A. Laso García, M. LaBerge, R. Zgadaj, A. Köhler, J. P. Couperus Cabadağ, O. Zarini, T. Kurz, A. Ferrari, M. Molodtsova, L. Naumann, T. E. Cowan, U. Schramm, A. Irman, and M. C. Downer, *Scientific Reports* **11**, 14368 (2021).
- ³²R. Behrens and P. Ambrosi, *Radiation Protection Dosimetry* **101**, 73 (2002).
- ³³C. D. Chen, J. A. King, M. H. Key, K. U. Akli, F. N. Beg, H. Chen, R. R. Freeman, A. Link, A. J. Mackinnon, A. G. MacPhee, P. K. Patel, M. Porkolab, R. B. Stephens, and L. D. Van Woerkom, *Review of Scientific Instruments* **79**, 10E305 (2008).
- ³⁴F. Albert, B. B. Pollock, J. L. Shaw, K. A. Marsh, J. E. Ralph, Y.-H. Chen, D. Alessi, A. Pak, C. E. Clayton, S. H. Glenzer, and C. Joshi, *Physical Review Letters* **111**, 235004 (2013), publisher: American Physical Society.
- ³⁵A. Henderson, E. Liang, N. Riley, P. Yepes, G. Dyer, K. Serratto, and P. Shagin, *High Energy Density Physics* **12**, 46 (2014).
- ³⁶F. Horst, G. Fehrenbacher, T. Radon, E. Kozlova, O. Rosmej, D. Czarnecki, O. Schrenk, J. Breckow, and K. Zink, *Nuclear Instruments and Methods in Physics Research Section A: Accelerators, Spectrometers, Detectors and Associated Equipment* **782**, 69 (2015).
- ³⁷Y. J. Rhee, S. M. Nam, J. Peebles, H. Sawada, M. Wei, X. Vaisseau, T. Sasaki, L. Giuffrida, S. Hulin, B. Vauzour, J. J. Santos, D. Batani, H. S. McLean, P. K. Patel, Y. T. Li, D. W. Yuan, K. Zhang, J. Y. Zhong, C. B. Fu, N. Hua, K. Li, Y. Zhang, J. Q. Zhu, I. J. Kim, J. H. Jeon, T. M. Jeong, I. W. Choi, H. W. Lee, J. H. Sung, S. K. Lee, and C. H. Nam, *Laser and Particle Beams* **34**, 645 (2016), publisher: Cambridge University Press.
- ³⁸V. Stránský, V. Istoksaia, R. Versaci, L. Giuffrida, A. Cimmino, D. Margarone, and V. Olšovcová, *Journal of Instrumentation* **16**, P08060 (2021), publisher: IOP Publishing.

- ³⁹V. Istoksaia, V. Stránský, L. Giuffrida, R. Versaci, F. Grepl, M. Tryus, A. Velyhan, R. Dudžák, J. Krása, M. Krupka, S. Singh, D. Neely, V. Olšovcová, and D. Margarone, *Journal of Instrumentation* **16**, T02006 (2021).
- ⁴⁰National Institute of Standards and Technology, “X-Ray Mass Attenuation Coefficients - Plastic Scintillator,” (2023).
- ⁴¹Advatech UK Ltd, “YAG:Ce Scintillator Crystal,” (2023).
- ⁴²National Institute of Standards and Technology, “X-Ray Mass Attenuation Coefficients - Cesium Iodide,” (2023).
- ⁴³C. Ahdida, D. Bozzato, D. Calzolari, F. Cerutti, N. Charitonidis, A. Cimmino, A. Coronetti, G. L. D’Alessandro, A. Donadon Servelle, L. S. Esposito, R. Froeschl, R. García Alía, A. Gerbershagen, S. Gilardoni, D. Horváth, G. Hugo, A. Infantino, V. Kouskoura, A. Lechner, B. Lefebvre, G. Lerner, M. Magistris, A. Manousos, G. Moryc, F. Ogallar Ruiz, F. Pozzi, D. Prelicean, S. Roesler, R. Rossi, M. Sabaté Gilarte, F. Salvat Pujol, P. Schoofs, V. Stránský, C. Theis, A. Tsinganis, R. Versaci, V. Vlachoudis, A. Waets, and M. Widorski, *Frontiers in Physics* **9** (2022).
- ⁴⁴G. Battistoni, T. Boehlen, F. Cerutti, P. W. Chin, L. S. Esposito, A. Fassò, A. Ferrari, A. Lechner, A. Empl, A. Mairani, A. Mereghetti, P. G. Ortega, J. Ranft, S. Roesler, P. R. Sala, V. Vlachoudis, and G. Smirnov, *Annals of Nuclear Energy Joint International Conference on Supercomputing in Nuclear Applications and Monte Carlo 2013, SNA + MC 2013. Pluri- and Trans-disciplinarity, Towards New Modeling and Numerical Simulation Paradigms*, **82**, 10 (2015).
- ⁴⁵V. Vlachoudis, “Flair: A powerful but user friendly graphical interface for FLUKA,” (2009), pages: 790-800.
- ⁴⁶J. Ferri, *Étude des rayonnements Bétatron et Compton dans l’accélération d’électrons par sillage laser.*, phdthesis, Université Paris Saclay (COMUE) (2016).